Nanoscale Res Lett (2007) 2:496–503
DOI 10.1007/s11671-007-9088-y

NANO EXPRESS

# Facile Hydrogen Evolution Reaction on $WO_3$ Nanorods

**Janarthanan Rajeswari · Pilli Satyananda Kishore · Balasubramanian Viswanathan · Thirukkallam Kanthadai Varadarajan**

Received: 13 April 2007 / Accepted: 10 August 2007 / Published online: 1 September 2007


**Abstract** Tungsten trioxide nanorods have been generated by the thermal decomposition (450 °C) of tetrabutylammonium decatungstate. The synthesized tungsten trioxide ($WO_3$) nanorods have been characterized by XRD, Raman, SEM, TEM, HRTEM and cyclic voltammetry. High resolution transmission electron microscopy and X-ray diffraction analysis showed that the synthesized $WO_3$ nanorods are crystalline in nature with monoclinic structure. The electrochemical experiments showed that they constitute a better electrocatalytic system for hydrogen evolution reaction in acid medium compared to their bulk counterpart.

**Keywords** Tungsten trioxides · Thermal decomposition · Nanorods · Hydrogen evolution reaction · Electrocatalyst

## Introduction

One-dimensional (1D) nanostructures such as nanorods, nanowires and nanotubes have attracted attention due to their novel physical and chemical properties as well as their potential use in a wide range of advanced applications in the past decade [1, 2]. As a consequence, many synthetic methods have been developed to prepare various 1D nanostructures [3–6]. Of particular interest is the preparation of 1D nanostructure of tungsten trioxides ($WO_3$) and its suboxides ($WO_{3-x}$). $WO_3$ is used extensively as materials for electrochromic devices [7–10], gas sensors [11, 12], catalysts [13, 14] and secondary batteries [15]. Several synthetic approaches including electrochemical techniques, sonochemical approach, template mediated synthesis, bioligation, hydrothermal, wet organic and inorganic routes and thermal methods have been reported to fabricate $WO_3$ nanorods [16–51]. A method for the synthesis of tungsten oxide nanorods with planar defects or textured structure has been introduced by Zhang et al. and this method involves growth of $WO_{3-x}$ nanorods on the tips of electrochemically etched tungsten filament [16]. However, synthesis of such structure has been possible only in the presence of $H_2$ atmosphere. The nanorods of $WO_3$ have also been obtained by sonochemical method wherein Koltypin et al. have synthesized a mixture of $WO_2$–$WO_3$ nanorods by ultrasound irradiation of $W(CO)_6$ in diphenylmethane [17]. Tungsten oxide nanorods could also be obtained from templated route by using CNTs and colloidal gas aphrons as templates [18–20]. Therese et al. have adopted an organic amine assisted low temperature hydrothermal route for the synthesis of hexagonal $WO_3$ nanorods [23]. Inorganic compounds such as $Na_2SO_4$, $Rb_2SO_4$ and $K_2SO_4$ have been demonstrated as structure directing agents for the hydrothermal synthesis of 1-D $WO_3$ nanorods by Gu et al., Lu et al. and Xiao et al. [24–26]. Srivastava et al. have reported sol–gel followed by dip coating to produce $WO_3$ nanorods [28]. By altering the composition and concentration of solvent, it was shown that different morphologies and phases of $WO_3$ nanorods can be achieved [29]. However, all of these reported efforts involve multistep processes and limited to the use of directing agents such as CNTs and $M_2SO_4$ (M = Na, Rb and K). Hence, the synthesis would be tedious and requires careful removal of the structure directing agents to avoid contaminants. Moreover, sol–gel and hydrothermal

J. Rajeswari · P. S. Kishore · B. Viswanathan (✉) · T. K. Varadarajan
Department of Chemistry, National Centre for Catalysis Research, Indian Institute of Technology Madras, Chennai 600 036, India
e-mail: bvnathan@iitm.ac.in

methods proceed with a low yield. In order to overcome the difficulties mentioned, thermal method has been employed widely for the large scale synthesis of tungsten oxide nanorods/nanowires as they are simple, easy and free from catalysts and contaminants. Heat treatment of tungsten metal, such as, tungsten foil or tungsten filament heated at 800–1,600 °C [40–42], tungsten powder heated at 950 °C under the Ar gas flow on ITO glass/tungsten substrate at 900–1,100 °C [44], thermal evaporation of tungsten powder [45] and tungsten hexacarbonyl heated at 700 °C [39] have yielded 1-D $WO_3$ nanorods. All the above thermal methods related to 1-D tungsten oxide formation from the gaseous phase (vapor deposition) or thermal evaporation techniques are technically complex, require high temperature, harsh growth conditions, expensive experimental setup and complicated control processes. Recently, the single source molecular precursor route has opened a useful way for the synthesis of $WO_3$ nanorods/nanowires by thermal decomposition method [49–51]. It offers the distinct advantage of simplified fabrication procedure and equipment as compared with the thermal evaporation or vapor deposition methods. However, multiple steps for the synthesis of both precursor and 1-D $WO_3$, longer reaction time for precursor (6 days or 10 h) and relatively higher pyrolysis temperature (750 °C) were required. In this report, a facile synthesis of $WO_3$ nanorods based on the thermal decomposition of tetrabutylammonium decatungstate has been described. The method has several unique advantages. Firstly, it has been possible to obtain high yields of $WO_3$ nanorods at a relatively low temperature (450 °C) and short reaction time as compared to previously reported methods involving high temperature (≥700 °C). Secondly, different morphologies of the material (nanosheets and nanorods) can be achieved by altering the pyrolysis time. Moreover, the method followed for the synthesis of precursor is a simple precipitation which does not require any tedious experimental set up or does not consume much time when compared to the other methods. Finally, it is a generic method which can be applied for synthesis of other metal oxides such as $MoO_x$ and $V_2O_5$ by suitably altering the metal in the precursor.

There has been a continuous interest in studying the dimensionality-dependent properties of $WO_3$ and ultimately to fabricate nanodevices. Wang et al. have shown high Li intercalation capacity (1.12 Li per formula unit) for $WO_3$ nanorods than its bulk counterpart (0.78 Li per formula unit) [31]. The enhanced electrochemical performance has been attributed to the unique rod-like structure combined with increased edge and corner effects. Non stoichiometric $WO_{2.72}$ nanorods are found to function as sensors with extraordinary sensing ability and the activity has been attributed to the very small grain size and high surface to volume ratios associated with the nanorods [43]. Liu et al. have exhibited low turn on field for electronic emission by $WO_{2.9}$ nanorods [46]. Photoluminescent emission spectrum of tungsten oxide nanorods was found to show an additional blue emission peak at 437 nm than its bulk system [30]. All these results show the unique properties of $WO_3$ nanorods in comparison to their bulk counterpart. Similar enhanced activity can be expected for $WO_3$ nanorods in hydrogen evolution reaction. The aim of the current study is to verify such a supposition experimentally which is significant in the development of electrodes for electrochemical hydrogen production.

In recent years, hydrogen, in combination with fuel cells, has been proposed as a major alternative energy source. It provides energy at less environmental damage, with greater efficiency and acceptable cost compared to the conventional fossil fuels. Electrochemical production is one of the possible methods for hydrogen production. Materials such as Raney Ni, Ni–Mo and noble metals such as Pt, Pd and Ru have been employed for this purpose [52–55]. Inspite of their high catalytic activity for hydrogen evolution reaction, the process involving Pt and Pd are not commercialized due to their high cost and low abundance. This has lead to the investigation of newer materials or reduction of the loading of noble metals. Savadogo et al. have shown the HER using nickel electrodes with phosphotungstic acid. It has been demonstrated that the presence of W in the form of $WO_3$ in the polyoxometalates enhanced the electrocatalytic activity for hydrogen evolution [56, 57]. Baruffladi et al. have shown electrodeposited composites of non-stoichiometric tungsten oxides and either $RuO_2$ or $IrO_2$ to catalyze the hydrogen evolution in acid medium [58]. Platinum when supported on tungsten trioxide showed electrocatalytic activity for HER due to the synergism towards reactions in acid involving hydrogen atoms [59]. All these results show the significance of $WO_3$ in hydrogen evolution reaction.

In this article, we report a surfactant directed large scale synthesis of monoclinic $WO_3$ nanorods. This has been achieved by a simple pyrolysis of a single source precursor which consists of surfactant encapsulated tungsten oxide clusters. The employed route is template free, contaminant free, easy, economical and requires a low temperature for the fabrication of $WO_3$ nanorods. The morphology, chemical composition and structure were characterized by Scanning Electron Microscopy (SEM), Transmission Electron Microscopy (TEM), High resolution transmission electron microscopy (HRTEM) and X-ray diffraction (XRD). The as-synthesized tungsten trioxide nanorods have been employed as an electrocatalyst for hydrogen evolution reaction (HER). The electrocatalytic activity of the material for HER was investigated by cyclic voltammetry, linear sweep voltammetry and Tafel plots. The activity was compared with that of commercially obtained

bulk tungsten trioxide. Enhanced catalytic activity has been observed for $WO_3$ nanorods compared to bulk $WO_3$ as an electrocatalyst for HER.

## Experimental

### Materials

The commercial tungsten trioxide was purchased from Alfa Aesar. All other chemicals were purchased from Sisco Research Laboratories Pvt. Ltd and used as received.

### Preparation of Tungsten Trioxide Nanorods

Tungsten trioxide nanorods have been synthesized by using tetrabutylammonium decatungstate as the precursor material. The starting material was prepared according to the work described elsewhere [60]. The typical procedure involved the precipitation of tetrabutylammonium decatungstate by adding an aqueous tetrabutyl ammonium bromide solution to a clear yellow solution of tungstic acid preformed using sodium tungstate and concentrated hydrochloric acid. The white precipitate was washed with boiling water and ethanol, filtered, dried and then recrystallized in hot dimethyl formamide to give yellow crystals. The thermogravimetric analysis revealed that the tetrabutylammonium cation content in the compound is 29.0% (theoretical value: 29.2%) and the decomposition temperature is around 450 °C as reported [60]. The synthesis of tungsten trioxide ($WO_3$) nanorods from tetrabutylammonium decatungstate ($((C_4H_9)_4N)_4W_{10}O_{32}$) is carried out as follows: The precursor compound (1 g) was taken in an alumina or quartz boat and loaded inside a tubular furnace and heated at 450 °C at a heating rate of 25 °C per min under Ar atmosphere for 3 h. This was followed by gradual cooling to room temperature to obtain a blue powder of $WO_3$ nanorods. The total yield of the obtained material was 71% by weight (relative to the starting material). To further investigate the role of tetrabutylammonium (TBA) group on the morphology of $WO_3$, an experiment has been carried out in the absence of tetrabutylammonium ion. To achieve this, $(NH_4)_{10}H_2W_{12}O_{42} \cdot XH_2O$ has been taken as the precursor and pyrolysed under similar experimental conditions that were employed for the formation of $WO_3$ nanorods.

### Structural Characterization

X-Ray Diffraction (XRD) patterns were obtained by a powder diffractometer (XRD - SHIMADZU XD-D1) using a Ni-filtered CuKα X-ray radiation source. CRM 200 Raman spectrometer was employed, using the 514.5 nm line of an Ar ion laser as the excitation source. The morphology of the $WO_3$ nanorods was investigated by a scanning electron microscopy (SEM) (FEI, Model: Quanta 200). Transmission electron microscopy (TEM), Electron diffraction and Energy Dispersive X-ray Analysis (EDAX) were performed on a Philips CM12/STEM instrument. High-resolution Transmission Electron Microscopy (HRTEM) was carried out on a JEOL 3010.

### Electrochemical Characterization

A three electrode cell consisting of the glassy carbon as working electrode (0.07 $cm^2$), Pt wire and Ag/AgCl (satd. KCl) electrodes as counter and reference electrodes respectively were used. All electrochemical measurements were performed using a CHI660A potentiostat/galvanostat. The working electrodes for electrochemical measurements were fabricated by dispersing 5 mg of the catalyst in 100 μL of deionized water by ultrasonication for 20 min. From this dispersion 10 μL has been taken and placed on a glassy carbon electrode. The solvent was slowly evaporated by placing the electrode in an oven at 70 °C. Five microliter of nafion solution has been coated on the electrode as a binder and dried at room temperature. One molar $H_2SO_4$ was used as the electrolyte. The electrolyte solution was deaerated with high purity $N_2$ (99.99%) for 30 min before the electrochemical measurements.

## Results and Discussion

A schematic representation of the formation of $WO_3$ nanorods is shown in Fig. 1. It shows the possible mechanism of tungsten trioxide nanorods formation. The

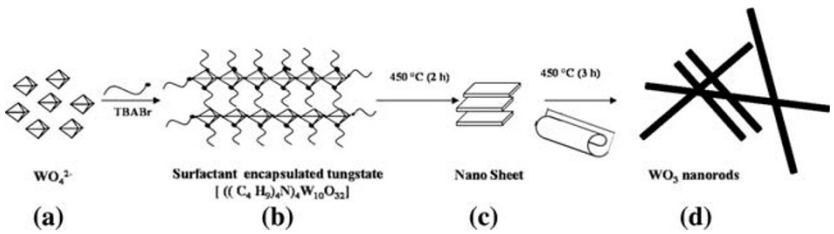


**Fig. 1** Scheme for the formation of $WO_3$ nanorods

precursor material is composed of the cationic surfactant group (tetrabutyl ammonium ion) and the anionic decatungstate ion, represented as octahedral units [60]. Formation of the precursor can be understood as follows: The $TBA^+$ cations react with the tungsten oxide octahedra (Fig 1a) and forms lamellar aggregates (also supported from the SEM image Fig 3a) of the $((C_4H_9)_4N)_4W_{10}O_{32}$ in which the tungstate anions are encapsulated in the array of TBA groups. The TBA groups are suggested to behave as glue that holds the $WO_6$ octahedra together with spacing between different lamellar layers (Fig 1b). In the crystallization process, surfactant molecules may serve as a growth controller, as well as an agglomeration inhibitor, by forming an encapsulated layer. When heated at 450 °C for 2 h, the structure directing, tetrabutylammonium group decomposes resulting in the formation of lamellar sheets of $WO_3$ (Fig 1c). On gradual increase of the pyrolysis duration to 3 h these lamellar sheets were rolled onto themselves to form $WO_3$ nanorods (Fig. 1d). The presence of tetrabutylammonium group in the precursor plays a vital role in the formation of nanorods. The hydrophilic head group of the surfactant binds to the $W_{10}O_{32}^{4-}$ anions. During this process the hydrophobic tail groups form a shield outside the anionic octahedra which prevents their agglomeration. The presence of the surfactant coating is of key importance not only for hydrophilic stabilization of the octahedra, but also for controlling long range self-assembly in concentrated dispersions.

Figure 2a shows the XRD recorded for $WO_3$ nanorods synthesized by a single step pyrolysis of tetrabutylammonium decatungstate. All the peaks can be undisputedly indexed to monoclinic $WO_3$ (JCPDS: 75–2072). There are no peaks detected for other phases, indicating that single phase of $WO_3$ with high purity has been prepared. No peaks of impurities were detected from this pattern. The average crystallite sizes of the nanorods was calculated by using Scherrer's formula

$$L = 0.89\,\lambda/\beta\cos\theta,$$

where, $L$ is the average crystallite size, $\lambda$ = 0.15418 nm for CuKα, $\beta$ is the half maximum peak width and $\theta$ is the diffraction angle in degrees. The average crystallite sizes calculated by the Scherrer's formula along the (001), (020), (200), (021) and (220) have values of about 36, 27, 34, 39 and 33 nm, respectively. The Raman spectrum (Fig. 2b) for the material shows characteristic O–W–O bending (260 and 334 $cm^{-1}$) and stretching modes (703 and 813 $cm^{-1}$) of $WO_3$. The typical morphology of the precursor compound, tetrabutylammonium decatungstate, $((C_4H_9)_4)N)_4W_{10}O_{32}$ and the as synthesized $WO_3$ are presented in the SEM images (Fig. 3a, b, respectively). Figure 3a displays the side view of the precursor

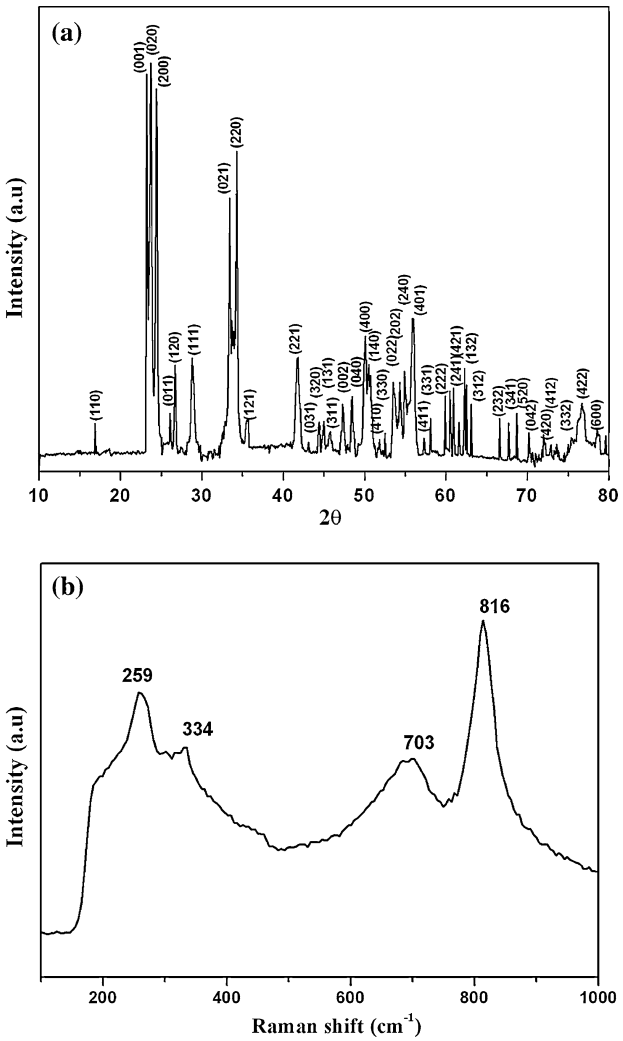


**Fig. 2** (**a**) Powder X-ray diffraction pattern and (**b**) Raman spectrum of $WO_3$ nanorods

compound revealing a lamellar aggregations. Figure 3b presents the image of the as synthesized $WO_3$ showing the formation of nanorods. The rods are polydispersed with few hundred nanometers (100–500 nm) of length and 20–60 nm of width. Thus the findings indicate that the pyrolysis products are obtained from the $((C_4H_9)_4)N)_4W_{10}O_{32}$ microsheets and the synthesized material constitutes nanosized one dimensional tungsten oxide materials. Figure 3c displays the SEM image of the $WO_3$ obtained from the pyrolysis of ammonium paratungstate, $(NH_4)_{10}H_2W_{12}O_{42} \cdot XH_2O$. It can be seen that the material is composed of irregular particles of varying size with plate like morphology. From the SEM analysis, it is revealed that rod like morphology can be obtained only when tetrabutylammonium group is present in the precursor compound. SEM has also been employed to observe the morphology of the commercially obtained $WO_3$ (Fig 3d). It shows agglomerated microparticles with

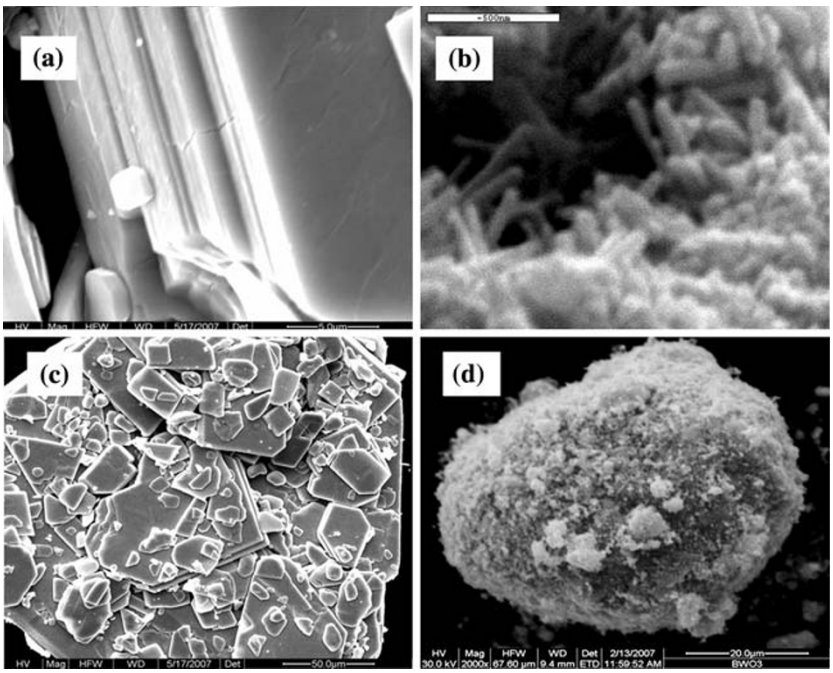


**Fig. 3** (**a**) SEM images of tetrabutylammonium decatungstate, (**b**) $WO_3$ nanorods obtained from the pyrolysis of tetrabutylammonium decatungstate, (**c**) $WO_3$ obtained from the pyrolysis of ammonium paratungstate and (**d**) commercially obtained $WO_3$

no specific morphology. TEM was also employed to provide further insight into structure and morphology of the as synthesized material. The morphologies of the products obtained after 2 h and 3 h were confirmed by the TEM images to be nanosheet (Fig. 4a) and nanorod (Fig. 4b, c), respectively. The sheet has a dimension of about 350 nm and 190 nm lateral size and thickness, respectively. The dimensions of the nanorods vary in ranges 130–480 nm and 18–56 nm of length and width, respectively. The high resolution TEM image of a nanorod is illustrated in Fig. 4d. The lattice fringes are explicitly clear with d spacing of 0.375 nm for the (020) plane. There has been a strong correlation on the d value obtained from the HRTEM and XRD. The electron diffraction shown in the inset of Fig. 4c indicates the crystallinity of the material. The EDAX (Fig. 5) results

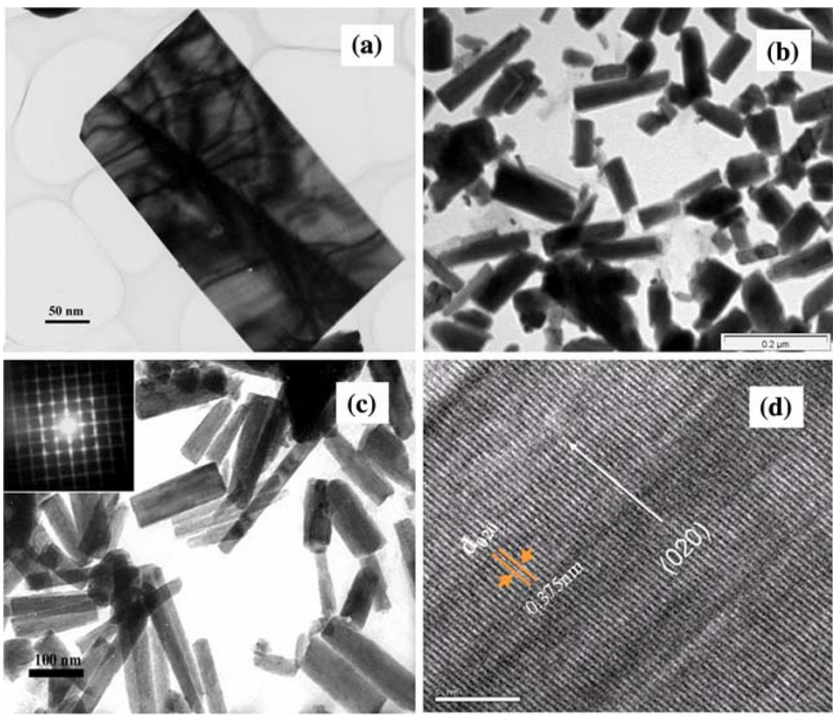


**Fig. 4** TEM images of $WO_3$ obtained from tetrabutylammonium decatungstate at various pyrolysis time. (**a**) 2 h and (**b**, **c**) 3 h, (**d**) HRTEM image of a $WO_3$ nanorods. Inset of Fig.4c Electron diffraction pattern of $WO_3$ nanorods

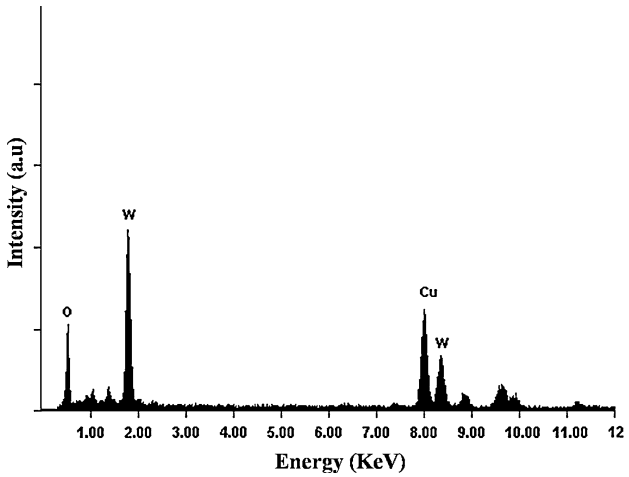


**Fig. 5** EDX spectrum of $WO_3$ nanorods

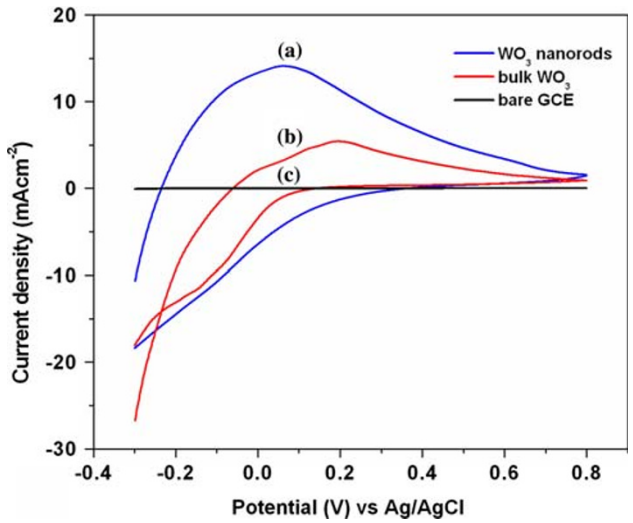


**Fig. 6** Cyclic voltammograms of (**a**) $WO_3$ nanorods, (**b**) bulk $WO_3$ and (**c**) bare glassy carbon electrode in 1 M $H_2SO_4$ at a scan rate of 25 mV $s^{-1}$

confirmed the presence of respective constituent elements in $WO_3$ nanorods. The copper signals originate from a copper supporting microgrid.

Tungsten trioxides in sulfuric acid medium form tungsten bronzes which are highly electron and proton conducting [61–63]. The redox processes involved in acid medium can be represented as follows: During the forward process represented in Eq. 1, $H_xWO_3$ (tungsten bronze) is formed and in the reverse process (Eq. 2), hydrogen is evolved.

$$xH^+ + xe^- + WO_3 \rightarrow H_xWO_3 \quad (1)$$

$$H_xWO_3 \rightarrow x/2H_2 + WO_3 \quad (2)$$

Figure 6a and b shows the cyclic voltammograms of $WO_3$ nanorods (as synthesized) and bulk $WO_3$ (commercial) respectively on glassy carbon electrode in 1 M $H_2SO_4$ at a scan rate of 25 mV $s^{-1}$. The bare glassy carbon electrode (GCE) shows no activity towards hydrogen evolution (Fig. 6c). $WO_3$ nanorods show a broad anodic peak at potential 0.1 V whereas the peak has shifted towards positive potential (0.2 V) for bulk $WO_3$. The anodic peak current density of $WO_3$ nanorods and bulk $WO_3$ are 14 mA $cm^{-2}$ and 5 mA $cm^{-2}$, respectively, at a scan rate of 25 mV $s^{-1}$. The current density for $WO_3$ nanorods is enhanced by 2.8 times to that of the bulk $WO_3$. The lower anodic peak potential and higher current density for $WO_3$ nanorods reveal the facile formation of tungsten bronzes in nanorods compared to the bulk material.

The stability of electrode in working electrolyte is one of the important properties when it is applied in industrial production [64]. CV is employed to investigate the stability of the electrode. Figure 7a and b shows the cyclic voltammograms of $WO_3$ nanorods and bulk $WO_3$ respectively in 1 M $H_2SO_4$ at a scan rate of 25 mV $s^{-1}$ for 50 consecutive cycles. For the $WO_3$ nanorods almost no activity variation was observed even after several cycles indicating its stability in sulfuric acid medium. Where as for the bulk $WO_3$, the peak current was observed to decrease as the cycle number increases. This shows the poor stability of bulk $WO_3$ in acid medium. This result is in agreement with

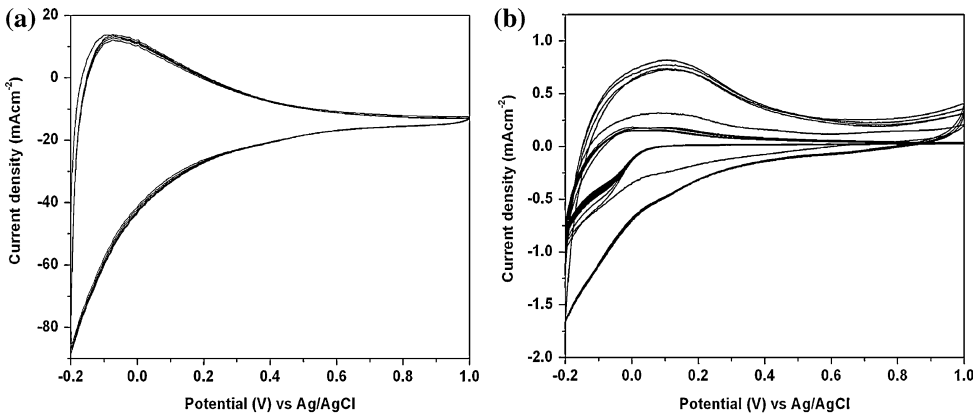


**Fig. 7** Cyclic voltammograms of (**a**) $WO_3$ nanorods and (**b**) bulk $WO_3$ for 50 cycles in 1 M $H_2SO_4$ at a scan rate of 25 mV $s^{-1}$

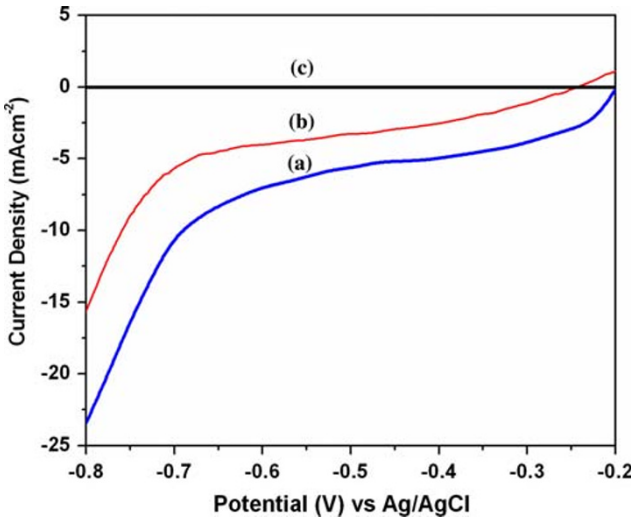


**Fig. 8** Linear sweep voltammograms of (**a**) $WO_3$ nanorods and (**b**) bulk $WO_3$ and (**c**) bare glassy carbon electrode in 1 M $H_2SO_4$ at a scan rate of 5 mV $s^{-1}$

the stability of the nanostructures of $WO_3$ described by Lee et al. [65] and Ganesan et al. [66]. It has been demonstrated that the nanoparticles of $WO_3$ and $WO_3$ microspheres exhibit excellent cycling stability in 1 M $H_2SO_4$ compared to the amorphous $WO_3$ films. The linear sweep voltammograms of $WO_3$ nanorods and bulk $WO_3$ carried out in 1 M $H_2SO_4$ at a scan rate of 5 mV $s^{-1}$ in the potential range –0.2 to –0.8 V are shown in Fig. 8a and b, respectively. The bare glassy carbon electrode showed no activity towards hydrogen evolution as evident from the Fig. 8c. At –0.8 V, the current densities of HER on $WO_3$ nanorods (23 mA $cm^{-2}$) is higher than that of bulk $WO_3$ (15 mA $cm^{-2}$) indicating the enhanced electrocatalytic activity of $WO_3$

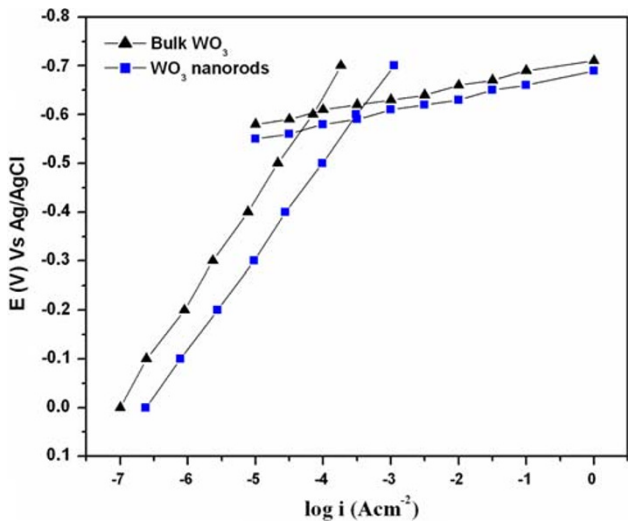


**Fig. 9** Tafel plots for HER on $WO_3$ nanorods and bulk $WO_3$ in 1 M $H_2SO_4$ at a scan rate of 2 mV $s^{-1}$

**Table 1** Electrochemical parameters of the HER obtained from the Tafel plots for different electrode materials

| Electrode | Slope, b (V $A^{-1}$ $cm^2$) | | $i_o$ (A $cm^{-2}$) |
|---|---|---|---|
| | Region 1 | Region 2 | |
| Bulk $WO_3$ | –213 | –30 | $8.57 \times 10^{-7}$ |
| $WO_3$ nanorods | –188 | –25 | $2.75 \times 10^{-6}$ |

nanorods. The kinetic parameters of the electrodes were determined from the Tafel plot as shown in Fig. 9 and the data are summarized in Table 1. The Tafel plots show two well-defined linear regions for both bulk $WO_3$ as well as $WO_3$ nanorods. The slopes in the low current density region (region 1) for bulk $WO_3$ and $WO_3$ nanorods are –213 and –188 mV $A^{-1}$ $cm^2$, respectively. The slopes are –30 and –25 mV $A^{-1}$ $cm^2$ in the high current density region for bulk $WO_3$ and $WO_3$ nanorods respectively (region 2). The lower Tafel slope obtained for $WO_3$ nanorods in comparison to bulk $WO_3$ indicates the facile HER on $WO_3$ nanorods as the electrode. The exchange current densities calculated at –0.199 V (Ag/AgCl (Satd KCl)) for 1 M $H_2SO_4$ solution provides information on the catalytic activity of the electrode for HER. The higher exchange current density value of $WO_3$ nanorods ($2.75 \times 10^{-6}$ A $cm^{-2}$) when compared to bulk $WO_3$ ($8.57 \times 10^{-7}$ A $cm^{-2}$) shows the better catalytic performance of $WO_3$ nanorods towards HER. The results can be attributed to the unique electrochemical behavior of 1-D nanostructures. 1-D nanostructures provide large electrode-electrolyte interface for the reaction to take place in a facile manner. Moreover, it has also been reported that the nanorod and nanowire form of the material is considered to influence its physical properties, which depart from the properties of their bulk phases due to the quantum effects related to the shape and size [67]. Thus it is demonstrated that improved HER activity can be achieved by using $WO_3$ nanorods as an electrocatalyst.

## Conclusions

In summary, we demonstrate a thermal decomposition method for the synthesis of 1-D $WO_3$ nanorods in high yield using a single source precursor. One of the important aspects of this method is the in situ formation of nanostructures due to the surfactant encapsulated metal oxide clusters. The advantage of this method is the tunability of the metal precursor and the surfactant group. This aspect of the method can be exploited for the synthesis of several other transition metal oxide nanorods. We have also synthesized nanorods of molybdenum oxide and mixed oxides of molybdenum and vanadium using similar strategy. The

as synthesized $WO_3$ nanorods perform well as an electrocatalyst with enhanced electrocatalytic activity for HER when compared to its bulk counterpart. The results show the possibility of minimizing the loading of noble metal electrocatalyst for HER by using $WO_3$ nanorods as catalyst support.

## References


1. S. Iijima, Nature **354**, 56 (1991)
2. M.H. Huang, S. Mao, H. Feick, H. Yan, Y. Wu, H. Kind, E. Weber, R. Russo, P. Yang, Science **292**, 1897 (2001)
3. Z. Kang, E. Wang, M. Jiang, S. Lian, Y. Li, C. Hu, Eur. J. Inorg. Chem. **2**, 370 (2003)
4. Y.N. Xia, J.A. Rogers, K.E. Paul, G.M. Whitesides, Chem. Rev. **99**, 1823 (1999)
5. X. Wang, J. Zhuang, Q. Peng, Y. Li, Nature **437**, 121 (2005)
6. V.F. Puntes, K.M. Krishnan, A.P. Alivisatos, Science **291**, 2115 (2001)
7. M. Andrei, A. Roggero, L.M.S. Passerini, Polymer **35**, 3592 (1994)
8. J.G. Zhang, D.K. Benson, C.E. Tracy, S.K. Deb, A.W. Czanderna, R.S. Crandall, J. Electrochem. Soc. **141**, 2795 (1994)
9. Y. Li, Y. Aikawa, A. Kishimoto, T. Kudo, Electrochim. Acta. **39**, 807 (1994)
10. W. Cheng, E. Baudrin, B. Dunn, J.I. Zink, J. Mater. Chem. **11**, 92 (2001)
11. H.M. Lin, C.M. Hsu, H.Y. Yang, P.Y. Lee, C.C. Yang, Sens. Actuators, B Chem. **22**, 63 (1994)
12. A.A. Tomchenko, I.L. Emelianov, V.V. Khatko, Sens. Actuators B Chem. **57**, 166 (1999)
13. W. Sun, L. Xu, Y. Chu, W. Shi, J. Colloid Interface Sci. **266**, 99 (2003)
14. J.H. Pan, W.I. Lee, Chem. Mater. **18**, 847 (2006)
15. B. Goldner, F.O. Arntz, T.E. Haas, Solar Energy Mater. Solar Cells **32**, 421 (1994)
16. H. Zhang, M. Feng, F. Liu, L. Liu, H. Chen, H. Gao, J. Li, Chem. Phys. Lett. **389**, 337 (2004)
17. Y. Koltypin, S.I. Nikitenko, A. Gedanken, J. Mater. Chem. **12**, 1107 (2002)
18. B.C. Satishkumar, A. Govindaraj, M. Nath, C.N.R. Rao, J. Mater. Chem. **10**, 2115 (2000)
19. N. Shankar, M.F. Yu, S.P. Vanka, N.G. Glumac, Mater. Lett. **60**, 771 (2006)
20. S.F. Abdullah, S. Radiman, M.A.Abd. Hamid, N.B. Ibrahim, Coll. Surf. A. **280**, 88 (2006)
21. J. Polleux, N. Pinna, M. Antonietti, M. Niederberger, J. Am. Chem. Soc. **127**, 15595 (2005)
22. J. Polleux, A. Gurlo, N. Barsan, U. Weimar, M. Antonietti, M. Niederberger, Angew. Chem. Int. Ed. **45**, 261 (2006)
23. H.A. Therese, J. Li, U. Kolb, W. Tremel, Solid State Sci. **7**, 67 (2005)
24. X.W. Lou, H.C. Zeng, Inorg. Chem. **42**, 6169 (2003)
25. Z. Gu, T. Zhai, B. Gao, X. Sheng, Y. Wang, H. Fu, Y. Ma, J. Yao, J. Phys. Chem. B. **110**, 23829 (2006)
26. Z. Xiao, L. Zhang, Z. Wang, Q. Lu, X. Tian, H. Zeng, Mater. Lett. **61**, 1718 (2007)
27. B.B. Lakshmi, P.K. Dorhout, C.R. Martin, Chem. Mater. **9**, 857 (1997)
28. A.K. Srivastava, S.A. Agnihotry, M. Deepa, Thin Solid Films **515**, 1419 (2006)
29. H.G. Choi, Y.H. Jung, D.K. Kim, J. Am. Ceram. Soc. **88**, 1684 (2005)
30. K. Lee, W.S. Seo, J.T. Park, J. Am. Chem. Soc. **125**, 3408 (2003)
31. Q. Wang, Z. Wen, Y. Jeong, J. Choi, K. Lee, J. Li, Nanotechnology **17**, 3116 (2006)
32. G. Gu, B. Zheng, W.Q. Han, S. Roth, J. Liu, Nano Lett. **2**, 849 (2002)
33. M. Gillet, R. Delamare, E. Gillet, J. Crystal Growth **279**, 93 (2005)
34. Z.W. Liu, Y. Bando, C.C. Tang, Chem. Phys. Lett. **372**, 179 (2003)
35. C. Klinke, J.B. Hannon, L. Gignac, K. Reuter, P. Avouris, J. Phys. Chem. B. **109**, 17787 (2005)
36. Y. Li, Y. Bando, D. Golberg, K. Kurashima, Chem. Phys. Lett. **367**, 214 (2003)
37. Y. Li, Y. Bando, D. Golberg, Adv. Mater. **15**, 1294 (2003)
38. M. Gillet, R. Delamare, E. Gillet, Eur. Phys. J. D **34**, 291 (2005)
39. B. Park, K. Yong, Surf. Rev. Lett. **12**, 745 (2005)
40. D.Z. Guo, K.Y. Zhang, A. Gloter, G.M. Zhang, Z.Q. Xue, J. Mater. Res. **19**, 3665 (2004)
41. Y. Shingaya, T. Nakayama, M. Aono, Sci. Tech. Adv. Mater. **5**, 647 (2004)
42. A. Rothschild, J. Sloan, R. Tenne, J. Amer. Chem. Soc. **122**, 5169 (2000)
43. Y.S. Kim, S.C. Ha, K. Kim, H. Yang, S.Y. Choi, Y.T. Kim, Appl. Phys. Lett. **86**, 213105 (2005)
44. C.C. Liao, F.R. Chen, J.J. Kai, Sol. Energy Mater. Solar Cells **90**, 1147 (2006)
45. Y. Baek, K. Yong, J. Phys. Chem. C **111**, 1213 (2007)
46. J. Liu, Z. Zhang, Y. Zhao, X. Su, S. Liu, E. Wang, Small **1**, 310 (2005)
47. Y. Baek, Y. Song, K. Yong, Adv. Mater. **18**, 3105 (2006)
48. W.B. Hu, Y.Q. Zhu, W.K. Hsu, B.H. Chang, M. Terrones, N. Grobert, H. Terrones, J.P. Hare, H.W. Kroto, D.R.M. Walton, Appl. Phys. A. **70**, 231 (2000)
49. S.V. Pol, V.G. Pol, G.A. Seisenbaeva, L.A. Solovyov, A. Gedanken, Inorg. Chem. **44**, 9938 (2005)
50. Y. Li, X. Li, Z.X. Deng, B. Zhou, S. Fan, J. Wang, X. Sun, Angew. Chem. Int. Ed. **41**, 333 (2002)
51. X.L. Li, J.F. Liu, Y.D. Li, Inorg. Chem. **42**, 921 (2003)
52. I. Paseka, Electrochim. Acta **47**, 921 (2001)
53. M.D. Curtis, M.D. McClain, Chem. Mater. **8**, 936 (1996)
54. M. Wu, P.K. Shen, Z. Wei, S. Song, M. Nie, J. Power Sources **166**, 310 (2007)
55. E. Fachinotti, E. Guerrini, A.C. Tavares, S. Trasatti, J. Electroanal. Chem. **600**, 103 (2007)
56. O. Savadogo, E. Ndzebet, J. Appl. Electrochem. **23**, 915 (1993)
57. O. Savadogo, Mater. Chem. Phys. **35**, 145 (1993)
58. C. Baruffaldi, S. Cattarin, M. Musiani, Electrochim. Acta **48**, 3921 (2003)
59. S.A. Abbaro, A.C.C. Tseung, D.B. Hibbert, J. Electrochem. Soc. **127**, 1106 (1980)
60. A. Chemseddine, C. Sanchez, J. Livage, J.P. Launay, M. Fournier, Inorg. Chem. **23**, 2609 (1984)
61. P.J. Kulesza, L.R. Faulkner, Colloid Surface **41**, 123 (1989)
62. B. Reichman, A.J. Bard, J. Electrochem. Soc. **126**, 2133 (1979)
63. B. Reichman, A.J. Bard, J. Electrochem. Soc. **127**, 647 (1980)
64. H. Zheng, J. Huang, W. Wang, C. Ma, Electrochem. Commun. **7**, 1045 (2005)
65. S.H. Lee, R. Deshpande, P.A. Parilla, K.M. Jones, B. To, A.H. Mahan, A.C. Dillon, Adv. Mater. **18**, 763 (2006)
66. R. Ganesan, J.S. Lee, J. Power Sources **157**, 217 (2006)
67. C.N.R. Rao, F.L. Deepak, G. Gundaih, A. Govindaraj, Prog. Solid. Chem. **31**, 5 (2003)